

Properties of the π^* and σ^* states of the chlorobenzene anion determined by electron impact spectroscopy

Tomáš Skalický, Christophe Chollet, Nicolas Pasquier and Michael Allan

Department of Chemistry, University of Fribourg, Ch. de Musée 9, CH-1700, Fribourg, Switzerland

The selectivity of vibrational excitation by electron impact has been used to unambiguously assign the negative ion states (resonances) of chlorobenzene and to settle a recent controversy on this subject. The excitation functions of the ring deformation vibrations exhibit bands in the 0.8–1.4 eV range, identifying them as temporary electron captures in the b_1 and $a_2 \pi^*$ orbitals. A broad band peaking at 2.6 eV appears in the excitation functions of the C–Cl stretch vibration but is missing in the excitation functions of the ring deformation vibrations, proving that it corresponds to a temporary electron capture in the $\sigma_{\text{C-Cl}}^*$ orbital. A more detailed insight into the properties of the potential surfaces of the anion is gained from the excitation functions of many vibrations, and from their comparison with anion potential curves based on the Koopmans theorem. Slopes of the potential curves in the Franck–Condon region reproduce well the observed intensities of totally symmetric vibrations. Strong excitation of out-of-plane vibrations, corroborated by the calculations, reveal vibronic coupling of the $b_1 \pi^*$ and the o^* anion states. The $a_2 \pi^*$ state and the o^* state are coupled by vibrations with a_2 symmetry. Excitation of in-plane non-totally symmetric vibrations (b_2) reveals vibronic coupling between the two π^* states b_1 and a_2 , which is also reproduced by the calculated potential curves. The results indicate that symmetry lowering induced by vibronic coupling provides the path for dissociation of the r^* states of the chlorobenzene anion.

Introduction

Dissociative electron transfer to halogenated aromatic hydrocarbons



is an important step in electrochemistry and in nucleophilic substitution^{1,2} and is as such of industrial and ecological relevance. The same reaction in the gas phase, the dissociative electron attachment (DEA) may serve as a prototype for the condensed phase reaction and is by itself important in low pressure plasmas.

The vertical electron attachment to chlorobenzene in the gas phase is endothermic. The electronic states of the negative ion intermediate involved in the dissociation have thus enough energy to spontaneously lose (detach) the extra electron, and are called temporary negative ions or resonances.⁴ Their energies in organic compounds can be determined by the electron transmission spectroscopy (ETS) where the resonances appear as variations of electron current transmitted through a chamber filled with a diluted gas.⁴ Burrow *et al.* have applied ETS to chlorobenzene and found a strong band at 0.7 eV, followed by a much weaker band at 1.15 eV.⁵ They argued that the two r^* states of the anion are nearly degenerate, lying near 0.7 eV, and that the 1.15 eV structure arises from a vibronic interaction between these two states. They further observed a broad band at 2.4 eV in the transmission spectrum and assigned it as a temporary occupation of the o^* orbital by analogy with a similar band in vinyl chloride. This assignment was supported by the calculation of the energies of the virtual orbitals and the application of the Koopmans theorem.⁶ The DEA spectrum of chlorobenzene has an intense Cl^- band near 1 eV.⁷ According to the above assignment this DEA must proceed via vibration-induced dissociation of the π^* states, the

direct dissociation being symmetry forbidden in the C_{2v} symmetry group. It can thus be viewed as an electron capture into a r^* orbital, followed by a vibration induced intramolecular electron transfer into a o^* MO and then by dissociation. This is in contrast to benzyl chloride, where the o^* orbital on the dissociating C–Cl bond is a part of the π^* orbital and a faster direct dissociation occurs.^{8–10}

Clarke and Coulson presented early potential curves for the chlorobenzene anion, pointed out the symmetry-forbidden nature of the dissociation and implied an energy barrier in the dissociation path.¹¹ The fact that the onset of the Cl^- dissociative electron attachment signal occurs at about the same energy as the first electron transmission band indicates, surprisingly, that in reality there is no such energy barrier. Asfandiarov *et al.*¹² estimated the predissociation rate in the presence of the barrier and argued that it can not be fast enough to explain the observed large DEA cross sections. As a possible explanation they then suggested that the assignment of the π^* and o^* states in chlorobenzene should be reversed, the resonance in the 0.7–1.15 eV range being o^* , so that direct dissociation is possible. This would imply that the Koopmans theorem fails in chlorobenzene. Modelli and Venuti subsequently used ETS measurements and theoretical calculations to defend the original assignment.¹³ The limitation of the ETS method is, however, that it provides no direct experimental indication of whether an anion state is o^* or r^* . A number of theoretical publications were concerned with the potential hypersurfaces of chlorobenzene and its anion. In a recent work Beregovaya and Shchegoleva¹⁴ calculated a number of local minima and saddle points on the anion hypersurface, considered several modes of vibronic coupling, and proposed an out-of-plane bend of the C–Cl bond as the primary way of mixing the $b_1 \pi^*$ and the $a_1 o^*$ states and providing a path towards dissociation with a very low or no barrier.

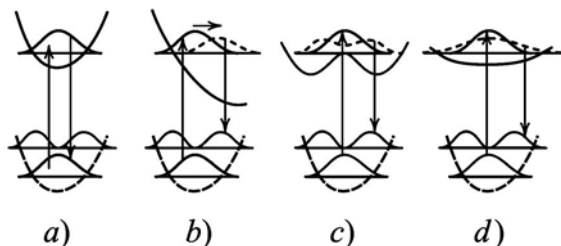


Fig. 1 Qualitative potential curves of a neutral molecule (dashed) and a short-lived anion (solid), illustrating the various methods of resonant vibrational excitation by electron impact. The ground state vibrational wave packet is promoted to the anion potential surface upon attachment of an electron (upward arrow). The packet then relaxes during the short lifetime of the anion. The relaxed wave packet (short dashes) is projected into various final vibrational states (downward arrow) upon the spontaneous electron detachment.

The present work uses the selectivity of resonant vibrational excitation to provide direct experimental evidence for the assignment of the observed resonances to the σ^* and the π^* states. It has been shown that vibrational excitation even in large polyatomic molecules can be very selective.¹⁵ The cross section (intensity) of the resonant excitation of a given vibration is related to the slope of the potential surface of the negative ion state in question with respect to the normal mode of that vibration.¹⁶ The selectivity of the vibrational excitation thus provides evidence of the bonding and antibonding properties of the temporarily occupied molecular orbital, providing a direct indication of the assignment, a method pioneered by Walker *et al.* in ethene.¹⁷ The mechanism of the resonant vibrational excitation is illustrated in Fig. 1. The attachment of an electron brings the nuclear wave packet to the potential surface of the anion, as indicated by the upward arrows. A repulsive anion potential, such as the case (b) in the figure, perturbs the nuclear wave packet during the short lifetime of the negative ion, resulting in a vibrationally excited neutral molecule after the detachment of the electron. Attachment of an electron into an MO which is neither bonding nor antibonding along a certain normal coordinate, resulting in a negative ion potential such as the case (a) in Fig. 1, does not lead to vibrational excitation, and the anion thus does not give rise to a band in the excitation function of this vibration. A repulsive potential is not the only possibility for vibrational excitation, however. Vibrational excitation is obtained also in the case of a double minimum potential such as the case (c), where the wave packet splits and flows down on the both slopes of the ridge. It even suffices when the anion potential is substantially flatter than the potential of the neutral molecule and the wave packet spreads during the lifetime of the resonance (case (d)). A very flat or double minimum shapes of potential curves are generally consequences of vibronic coupling, the role of which has been studied theoretically for temporary anions by Estrada *et al.*¹⁸ At first one may expect that only even quanta of vibrations are excited in cases (c) and (d) because the relaxed wave function remains totally symmetric. The breakdown of the Born–Oppenheimer approximation which accompanies the vibronic coupling causes the excitation of a single quantum and higher odd quanta as well, however.** The role of the intermediate negative ion in resonant vibrational excitation by electron impact resembles to some extent the role of the intermediate excited state in resonant Raman scattering.

The method of characterizing ground and excited states of anions by means of vibrational excitation functions suffered until recently from the fact that the relatively low resolution of the electron spectrometers did not suffice for the separation of the individual vibrations in larger molecules and the spectrometers often could not reach the very low energies where the negative ions of larger molecules are found. Progress has

2

recently been made in both aspects and the present study employs the improved instrumentation for a thorough study of the electronic states of the chlorobenzene anion. We first analyze the spectra using qualitative arguments, not relying on theory, in particular not relying on the use of the Koopmans theorem, to derive an assignment of the σ^* and π^* states of the anion. In a next step we derive more detailed information on the dynamics of the various states of the anion by comparing the observed excitation functions with potential curves based on the use of the Koopmans theorem. Finally, the dissociation channel of the π^* states of the anion is explored in light of the experimental results using the DFT/B3LYP model.

Experiment

The spectra were recorded with an electron spectrometer using electrostatic hemispherical analysers.^{19,20} The performance of this instrument has recently been improved—better compensation of residual electric fields in the collision region allows recording even at very low energies and the resolution is about 10 meV.²¹

The experiment has two steps. An electron energy loss spectrum is recorded first. In the present case the spectrum is recorded at a constant energy above the excitation thresholds, that is, the analyser is set to pass scattered electrons of a fixed residual energy E_r and the energy of the incident electrons is swept. The spectrum shows an overview of which vibrational states are excited, that is of the selectivity at the given (residual) electron energy. The details of the excitation process are measured in the second step, where the efficiency (cross section) for the excitation of a given vibration is recorded as a function of the incident electron energy E_i . Both the incident and the residual energies are swept, their difference being kept constant and equal to the energy of the vibrational state whose excitation function is recorded. Bands in such an excitation function correspond to states of the negative ion, more precisely to those states where the potential surface has a slope (or is otherwise distorted—see Fig. 1) with respect to the normal coordinate of the vibration being excited. A given state of a negative ion thus appears more or less strongly, or is even missing, in excitation functions of different vibrations. This additional information provides a 'tag' on each band, giving indication of the nature of the state.

The spectrometer has a small Wien filter in front of the detector, capable of separating scattered electrons and ions from DEA. Tuning this filter to pass ions permits recording of ion (in this case Cl^-) yields as a function of incident electron energy, that is, of dissociative attachment spectra.

All spectra were recorded at a scattering angle of 135° to reduce vibrational excitation due to the direct, dipole scattering, which peaks in the forward direction, and thus to enhance the resonant scattering, which is of interest here. The sample gas was introduced through a 250 μm diameter nozzle, whose temperature was about 30°C .

Results

Qualitative interpretation

Fig. 2 shows a typical electron energy loss spectrum, providing an overview of the vibrational states excited. It has been recorded at constant residual energy, all bands are recorded 0.8 eV above excitation thresholds. The incident energy varies, but remains within the 0.8–1.2 eV resonance region. The vibrational peaks are assigned and labeled according to the scheme of Whiffen,²² reproduced in Table 1. Closely spaced vibrations, for example a and c, k and l, can not be separated even with the present resolution, but this remaining band overlap does

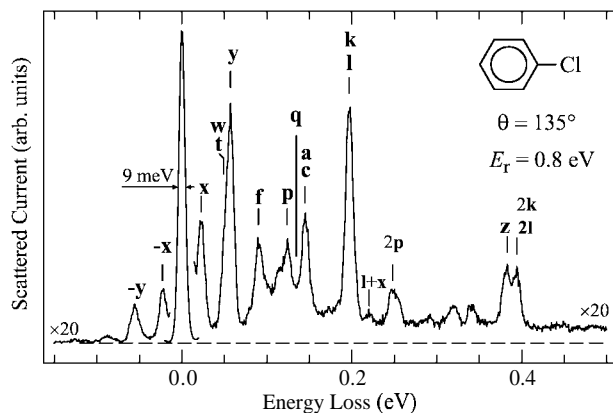


Fig. 2 Electron energy loss spectrum recorded with a constant residual energy of $E_r = 0.8$ eV. Energies of selected vibrational states (Table 1) are indicated above the spectrum. Superrelax peaks are seen to the left of the elastic peak.

Table 1 Experimental vibrational energies E , in meV, ordered according to the type of vibration (from Whiffen²²)

Type	Label	Symmetry	E
C-H stretch	z_1	a_1	381
	z_2	a_1	378
	z_3	a_1	376
	z_4	b_2	381
	z_5	b_2	378
C-C stretch	k	a_1	196
	l	b_2	196
	m	a_1	183
	n	b_2	179
C-H in-plane deformation	o	b_2	164
	e	b_2	158
	a	a_1	146
	c	b_2	144
	d	b_2	132
	b	a_1	127
Ring breathing	p	a_1	124
C-H out-or-plane derormation	j	b_1	122
	h	a_2	120
	i	b_1	112
	g	a_2	103
	f	b_1	92
	v	b_1	85
Ring out-or-plane derormation	w	a_2	50
	s	b_2	76
C-Cl stretch	q	a_1	135
	r	a_1	87
	t	a_1	52
C-Cl in-plane deformation	u	b_2	37
C-Cl out-or-plane derormation	y	b_1	58
	x	b_1	24

not prevent unambiguous assignment of resonances, as will be shown below.

Before discussing the selectivity of resonant vibrational excitation in more detail we should mention that, besides bands due to temporary attachment of an electron to virtual orbitals which represent the main subject of this work, one often finds strong enhancements of vibrational excitation in a narrow energy range just above the excitation threshold. These 'threshold peaks' were originally discovered in polar diatomic molecules²¹ and have subsequently often been studied. Their role in vibrational excitation of polyatomic molecules has been discussed in a recent paper on *cis*- and *trans*-difluoroethenes.²⁴

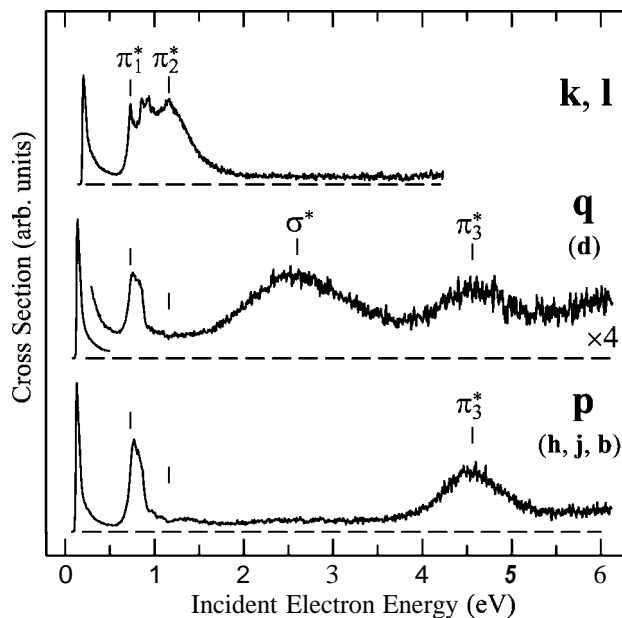


Fig. 3 Cross sections for exciting the vibrations p, q and (k,l) as indicated on the right. The vibrations given in parentheses lie close in energy and overlap partly with the main vibrations.

Threshold peaks are found in most of the excitation functions presented here, but will not be further discussed.

The selectivity of the resonant vibrational excitation is particularly well illustrated on the excitation functions of the vibrations (k,l), p and q, shown in Fig. 3. Vibration p is the totally symmetric (a_1) ring breathing and must be thus excited by temporary electron attachment to the π^* orbitals, located on the ring and antibonding with respect to the C-C bonds, but not by electron attachment to the σ^*_{C-Cl} orbital, which is located on the C-Cl bond. The vibration q is also totally symmetric but is, according to Whiffen,²² "X-sensitive" (where X is a halogen in a series of halobenzenes), meaning that it involves an appreciable amount of C-Cl stretch. It will therefore also be excited by temporary electron attachment to the σ^* orbital, located on, and antibonding with respect to, the C-Cl bond. The fact that the broad band peaking at 2.6 eV is prominent in the excitation of the vibration q but missing in the excitation of the vibration p identifies it positively as due to the σ^*_{C-Cl} state of the anion. The bands around 0.8 and 4.5 eV must be due to the π^* states of the anion.

The vibrations k and l overlap, and only the superposition of the excitation functions can be recorded. Both vibrations involve a C-C stretch and are located on the ring—it is not surprising that the σ^* band is missing in the excitation function. The low energy band is broader, however, indicating that both components of the π^* resonance cause vibrational excitation here. At the present qualitative stage of the argument it is not possible to decide which is which. A combined theoretical and experimental argument given below favors the ordering b_1 below a_2 , although this conclusion is, in contrast to the above assignment of the bands to π^* and σ^* states, not unambiguous.

The resulting assignment of the electronic states of chlorobenzene anion is given in Fig. 4. This assignment agrees in essential features with the conclusions of Modelli and Venuti.¹³ This means that the low energy reductive dissociation of chlorobenzene must be due to indirect dissociation of the π^* states, symmetry forbidden in the C_{2v} group, and not to direct dissociation of the σ^* state. It further means that chlorobenzene is no exception in terms of applicability of the Koopmans model with empirical scaling,²⁵ its predictions are correct within

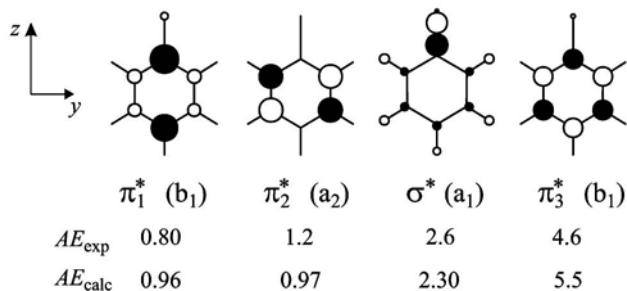


Fig. 4 Schematic diagrams of the orbitals temporarily occupied in the chlorobenzene negative ion. Vertical attachment energies AE , in eV, experimental and calculated using the Koopmans theorem with HF/6-31G* orbitals and the empirical scaling of ref. 25 are given.

about ± 0.3 eV for the three low-lying states, as in virtually all cases where it has been tested.

Potential curves

Encouraged by the qualitatively correct predictions made by the scaled Koopmans model we shall use it to calculate potential curves for the chlorobenzene anion and attempt to understand qualitatively the relative intensities of the anionic bands in the excitation spectra of various vibrations. As recently reiterated by Sommerfeld (on the analogous case of organic dianions),²⁶ the coupling to continuum makes the calculation of temporary anions much more difficult than the calculation of excited states of positive ions or neutral molecules. A correct treatment, even in the simplest form, the 'local complex potential' model, describes the potential by a real part, the energy, and an imaginary part, describing the strength of the coupling to the continuum, that is the autodetachment rate.²⁷ Both the real and the imaginary parts are a function of the nuclear coordinates. The local complex potential approximation fails to describe phenomena near the excitation threshold and even more elaborate 'nonlocal' models are then required.²⁸ The parameters of even the simpler local approximation can at present not be calculated *ab initio* for molecules of the size of chlorobenzene, however. We therefore revert to the Koopmans model with empirical scaling to approximate the real part of the potential curve which permits a qualitative correlation of observed band intensities with slopes of the potential curves.

We take the SCF energy as a function of the normal coordinate to approximate the potential curve of the neutral chlorobenzene and add the scaled virtual orbital energies to obtain the potential curves of the anion. This method neglects the core excited resonances. They may be expected at energies close to the energies of the excited states of chlorobenzene, around 4.6 eV,²⁹ that is above the energies of primary interest in this work. In fact, admixture of core excited configurations could be the reason why the Koopmans model works less well for the π_3^* state than for the lower lying states. The core excited resonances lead to only weak vibrational excitation (they appear more prominently in the excitation functions of electronically excited states, see the example of benzene³⁰ and their neglect is thus not a serious drawback for the present work. The Koopmans method takes into account vibronic coupling between the shape resonances, but neglects vibronic coupling with the core excited resonances, which may occur at higher energies. The exact result of the Koopmans model depends on the basis set and the empirical scaling parameters. For consistency with our earlier work we use the 6-31G* basis set and the scaling parameters of Chen and Gallup.²⁵ This choice leads to an artificial near degeneracy of the b_1 and a_2 π^* states (Fig. 4). The experiment indicates that in reality these two states are split by a small amount, although the observed splitting could be primarily of vibronic origin as discussed in more

4 detail below. The basis set choice of Modelli and Venuti gives a slightly larger splitting of 0.05 eV.¹³ The splitting is a result of two opposing effects, the inductive stabilization of the π^* MOs by the electronegative chlorine, whereby the b_1 MO is stabilized more since it has a large coefficient on the carbon adjacent to Cl, and the conjugative destabilization of the b_1 π^* MO by the occupied p_π orbitals on chlorine. The fact that the exact magnitude of the splitting and perhaps even the ordering of the states is not correctly reproduced by the calculation is thus understandable and not alarming. The near degeneracy of the Koopmans energies is misleading when observing the potential curves, however, and to improve clarity and to increase consistency with the experiment the b_1 energies are shown lowered by 0.04 eV and a_2 energies raised by 0.04 eV in all the curves in this work. Since the two states are strongly mixed by vibrations of b_2 symmetry, the choice of the ordering in the equilibrium geometry of chlorobenzene and the exact size of the splitting at this geometry do not affect the qualitative conclusions derived from the potential curves.

The vibrational modes were calculated within the density functional (DFT) B3LYP and the Hartree-Fock (HF) models for neutral chlorobenzene. The normal mode displacements represented as arrows³¹ are shown above the potential curves in the figures. They were extrapolated linearly for the calculation of the potential curves. The potential curves for the vibrations q and p , shown in Fig. 5, conform to the qualitative expectations described above. The σ^* potential curve has a steep slope in the Franck-Condon region for the mode q but mimics the ground state potential curve for the mode p , explaining the prominence of the σ^* band in the excitation function of the former, and its absence in the later mode. The slopes of the π^* potential curves are small for both the

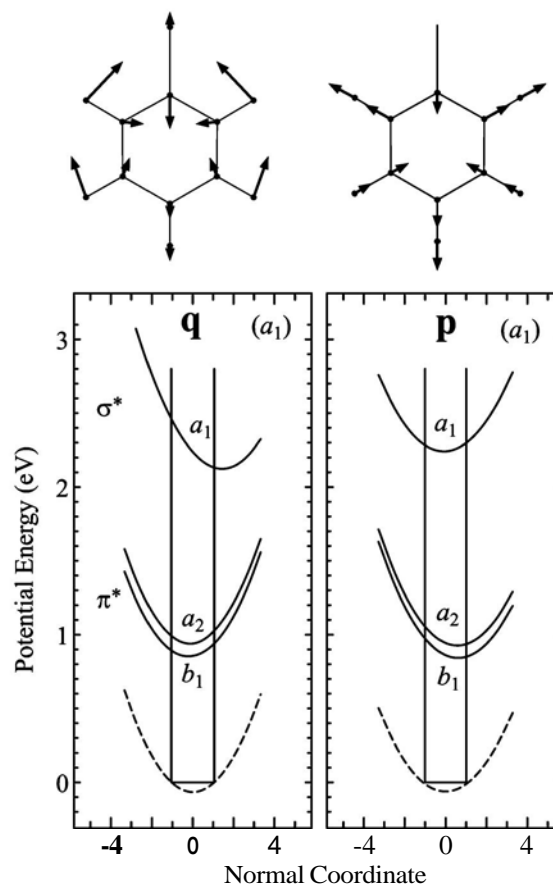


Fig. 5 Potential curves and normal modes for the vibrations q and p . The dashed curves refer to the ground state of neutral chlorobenzene, solid curves to the states of the negative ion.

p and y modes, explaining the weakness of the π^* bands in the excitation functions. The intensity of a band in the excitation function depends not only on the slope of the potential curve, but it also decreases with increasing autodetachment rate since short lifetime towards autodetachment does not allow substantial relaxation of the nuclear wave packet. The σ^* resonance has very short lifetime towards autodetachment because of its higher energy and involvement of lower partial waves. This explains why the σ^* band is completely absent in the excitation function of the p vibration, whereas the π^* band is weakly present even in the p and y excitation functions, despite the small slopes.

The potential curves for the vibrations k and l are shown in Fig. 6. The absence of the σ^* band in the corresponding excitation function of Fig. 3 is well explained—neither of the potential curves has an appreciable slope in the Franck–Condon region. The pronounced intensity of the π^* bands is also well rationalized. Both π^* potential curves have steep slopes for the mode k and are strongly distorted by vibronic coupling for the mode l—both circumstances lead to vibrational excitation. The b_2 vibration l couples the two components of the low-lying π^* resonance since $a_2 \otimes b_1 = b_2$. Drawings of the π^* molecular orbitals along the b_2 normal coordinate show that the two orbitals rotate by a substantial angle in function of the vibrational excursion. The electronic wave function thus vanes rapidly as a function of the nuclear coordinate, a circumstance characteristic of vibronic coupling and a prerequisite for a breakdown of the Born–Oppenheimer approximation. The overlap of the k and l vibrational bands does not, unfortunately, allow to see in the spectra which

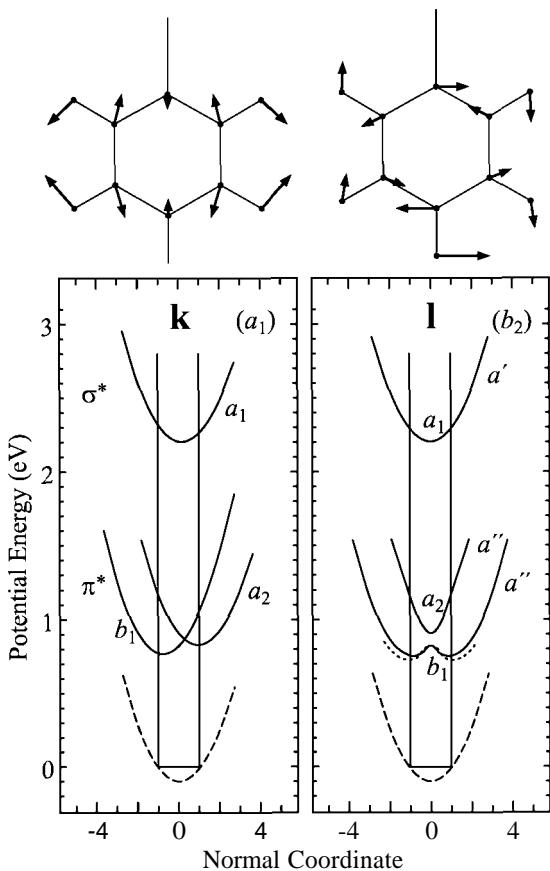


Fig. 6 Potential curves and normal modes for the vibrations k and l. The a' and a'' symmetry labels in the right panel refer to the anion distorted along the l normal mode, in the C_s symmetry group. The short dashed b_1 curve in the right panel has been obtained as the anion energy with the DFT/B3LYP model (shifted vertically to fit the vertical position of the Koopmans-model curve).

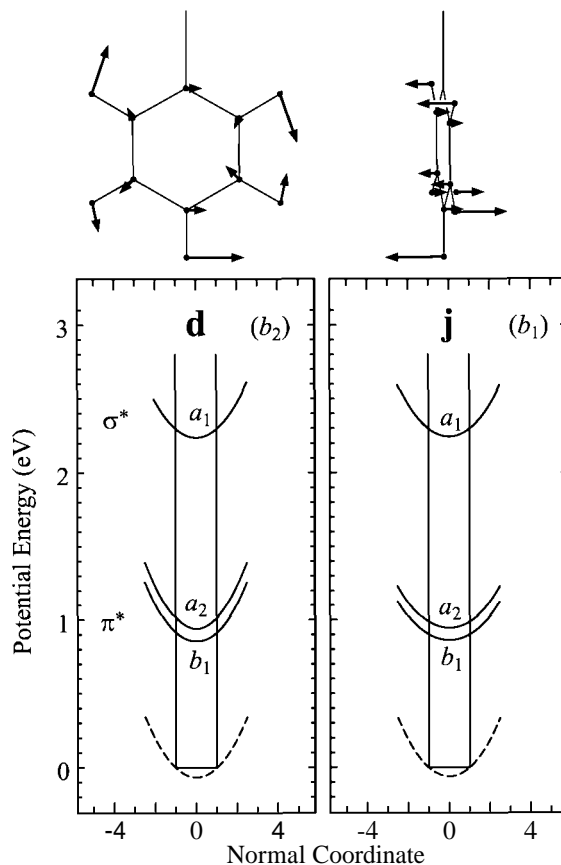


Fig. 7 Potential curves and normal modes for the vibrations d and j.

mechanism, slope along the mode k or vibronic coupling along the mode l, is more important. Fig. 7 shows the potential curves for the vibrations d and j which overlap to some degree with the vibrations q and p discussed above. All anion curves mimic the potential curve of the neutral chlorobenzene—these two vibrations are not expected to be significantly excited.

The vibrations x and y are very prominent in the energy loss spectrum of Fig. 2, surprisingly, because they are not totally symmetric and their excitation is not allowed by the first order symmetry selection rules.^{15,32} The excitation functions of Fig. 10 show that both vibrations are excited primarily by the lower of the two π^* resonances. Both vibrations are out-of-plane deformations with the symmetry b_1 , that is, they couple the b_1 π^* and the a_1 σ_{C-Cl}^* resonances. The effect of the vibronic coupling is clearly seen in the potential curves of Fig. 8. The ‘repulsion’ of the b_1 π^* and the a_1 σ_{C-Cl}^* potential curves for nonzero excursions along the x and y normal modes is not strong enough to cause a double minimum, but makes the b_1 π^* potential curve very flat, opening the possibility of vibrational excitation as in the case (d) of Fig. 1. The fact that it is the lower of the two π^* resonances which is more prominent in the spectra of Fig. 10 and that it is the b_1 π^* resonance which is affected by the vibronic coupling provides indication that the ordering of the π^* states is b_1 below a_2 in the equilibrium geometry of neutral chlorobenzene, and this ordering is therefore indicated in Fig. 4. Note that in particular the vibration x does not overlap with any other vibration and the effect of vibronic coupling is, in contrast to the case of the vibration l discussed above, seen unambiguously.

Fig. 9 shows the potential curves for the overlapping vibrations t and w. The σ_{C-Cl}^* potential curve has a large slope with respect to the normal mode t, rationalizing the intense σ^* band in the excitation function of Fig. 10. The vibration w couples the a_2 π^* and the a_1 σ_{C-Cl}^* resonances and one would expect

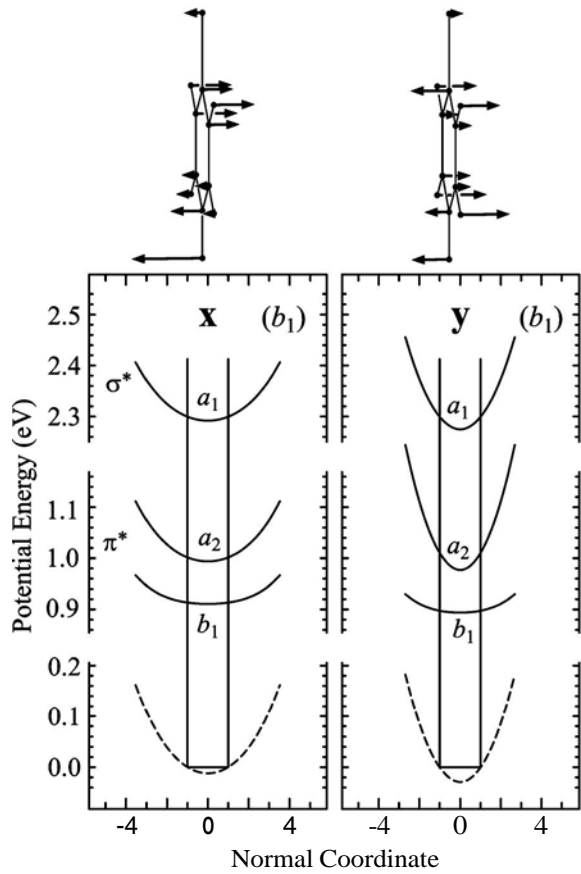


Fig. 8 Potential curves and normal modes for the vibrations x and y.

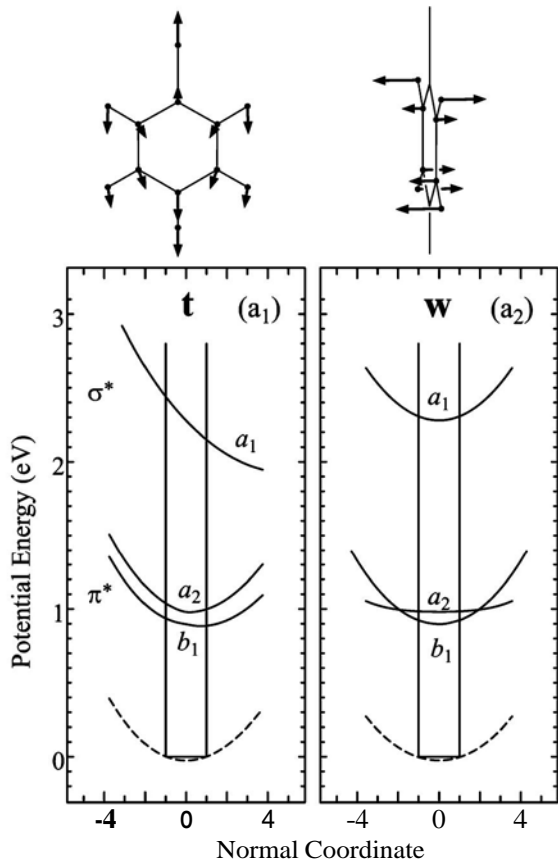


Fig. 9 Potential curves and normal modes for the vibrations t and w.

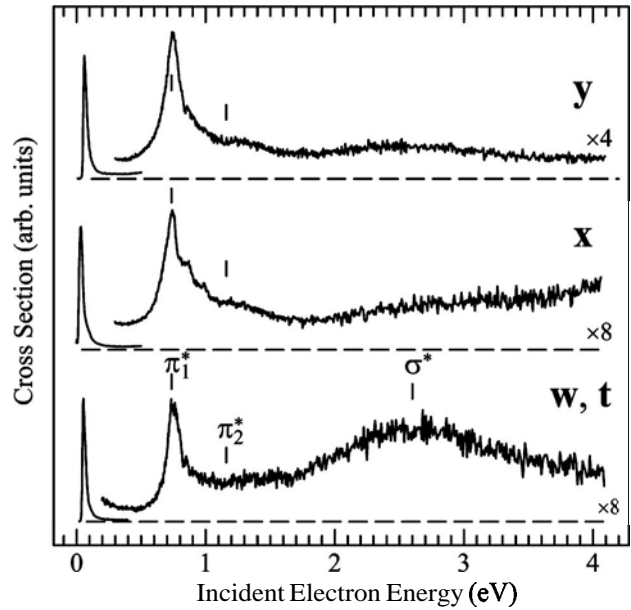


Fig. 10 Cross sections for exciting the vibrations indicated.

the $a_2 \pi^*$ band in the excitation function. The measured excitation curve does have some intensity in the 1–1.5 eV range, the signal does not have the form of a distinct band, however, because it connects to the σ^* band on the high energy side.

Figs. 11 and 12 show the excitation function and the potential curves for the overlapping vibrations a and c. Both the b_1 and the $a_2 \pi^*$ potential curves have some slope in the Franck-Condon region along the normal coordinate of a, in line with the fact that both bands at 0.8 eV and 1.2 eV are observed in the excitation function. Fig. 11 also shows the yield of Cl^- ions recorded with the same instrument by tuning the Wien filter to pass ions instead of electrons. The band is clearly broader than the π^* band in, for example, the excitation functions of the vibrations q, p or y, indicating that the upper branch of the π^* resonance is also involved. No two distinct bands can be discerned in the Cl^- yield spectrum, however. The onset of the Cl^- signal is more gradual than would correspond to the resolution of the instrument (around 7 meV in the incident beam), presumably because of hot bands. Thermal population

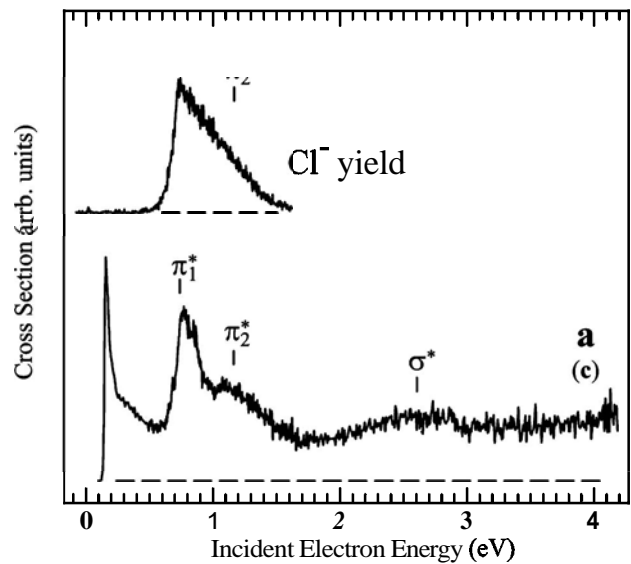


Fig. 11 Cross section for exciting the vibration a and the yield of Cl^- ions.

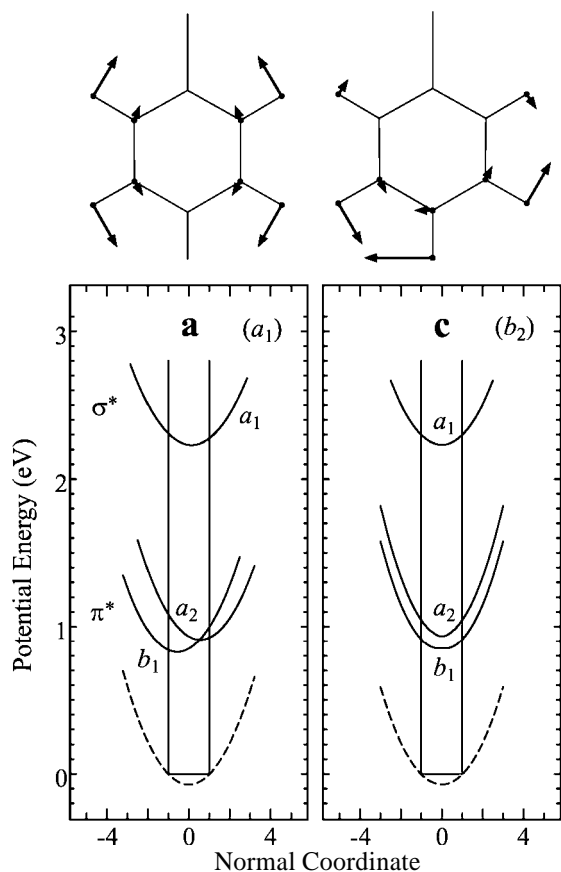


Fig. 12 Potential curves and normal modes for the vibrations a and c.

of low frequency non-totally symmetric vibrations is born out in the energy loss spectrum of Fig. 2. These vibrations are likely to enhance the DA cross section.

The study is concluded by two examples of excitation functions of overtone vibrations and the excitation function of the overlapping C–H stretch vibrations in Fig. 13. The σ^* band is seen in the excitation function of the 2q vibration and is absent in the excitation function of the 2p vibration, in analogy with

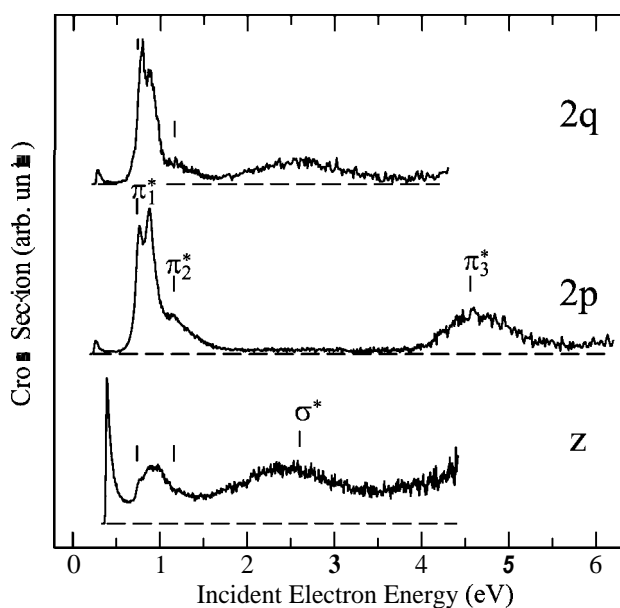


Fig. 13 Cross sections for exciting the vibrations indicated on the right.

the results for the corresponding fundamentals. The σ^* band is relatively weaker in comparison to the π^* band in the 2q excitation than in the 1q excitation, as is expected from the shorter autodetachment lifetime of the σ^* resonance. The σ^* band is prominent in the C–H excitation, in line with the expectation from the schematic diagram of the a_1 MO in Fig. 4, which shows that this MO is antibonding also with respect to the C–H bond lengths.

Finally, we carried out calculations on the chlorobenzene anion using the DFT/B3LYP model. As described for example in ref. 26 such calculations are in principle not admissible for temporary negative ions and rely on the fact that the outer electron is kept in the vicinity of the molecule artificially by the finite size of the basis set (basis set confinement). As a consequence, the calculated results are intruded by discretized continuum states and depend on the size of the basis set used. These problems are less serious for anion states at low energies, well below the pseudo-continuum states, and states where the coupling with the continuum is weak. This is the case for our π^* resonances, the weak coupling to continuum being revealed by the presence of vibrational structure in the lowest band in the spectra. We thus feel that the DFT model yields qualitatively correct results for the lowest electronic state of the anion, for which we use it. In addition, we use the DFT model to explore the dissociation coordinate and the anion becomes bound relatively soon when moving along this coordinate. Once the anion is bound, the calculation is justified.

We first addressed the question whether the shape of the potential hypersurface given by the DFT/B3LYP model agrees qualitatively with that given by the simple scaled Koopmans method. The comparison given in Fig. 6 confirms the qualitative agreement—both models indicate a curve with a shallow double minimum. (The absolute energy of the resonance is better reproduced by the Koopmans theorem with empirical scaling than by the energy difference of the anion and neutral molecule within the DFT/B3LYP model.)

We then explored the dissociation channel of the chlorobenzene anion and found a path leading without a noteworthy barrier towards a phenyl radical and Cl^- . The reaction coordinate involves an early pronounced symmetry lowering which mixes the π^* and the $a_1 \sigma_{\text{C-Cl}}^*$ states. Somewhat surprisingly, the most important aspect of this symmetry lowering, at least at an early stage of the dissociation and when starting with the a_2 state of the anion, appears to be twisting of the phenyl part of the molecule, particularly the hydrogen atoms, resembling closely the normal coordinate of the vibration w (Fig. 9). This distortion mixes the $a_2 \pi^*$ and the $a_1 \sigma_{\text{C-Cl}}^*$ MO's. The singly occupied molecular orbital (shown schematically in Fig. 14) then resembles a distorted $a_2 \pi^*$ MO (Fig. 4), strongly mixed with the $a_1 \sigma_{\text{C-Cl}}^*$ MO. The out-of-plane bending of the C–Cl bond, which mixes the $b_1 \pi^*$ and the $a_1 \sigma_{\text{C-Cl}}^*$ MO's and may intuitively be expected to be the primary mode of π^*/σ^* mixing, is calculated to be important in later stages of the dissociation.

Conclusions

The selectivity of vibrational excitation permits an unambiguous assignment of the electronic states of the chlorobenzene

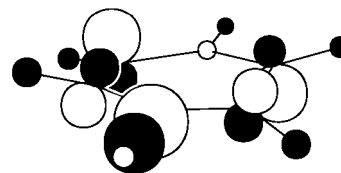


Fig. 14 Schematic diagram of the singly occupied orbital of the chlorobenzene negative ion in an early stage of dissociation.

anion already on a qualitative level of interpretation. The low-lying band in the 0.8–1.6 energy range, with vibrational structure, is assigned to the two π^* states. The broad structureless band peaking at 2.6 eV is due to the $\sigma_{\text{C-Cl}}^*$ state with a_1 symmetry. It is noteworthy that the present assignment does not depend on theoretical calculations. This assignment agrees with the earlier assignment of the ETS spectra^{5, 8} and confirms that the conclusions obtained from the application of the Koopmans theorem are correct.

Having verified the validity of the Koopmans model as far as the ordering of the π^* and σ^* states is concerned, we used it to calculate potential curves of chlorobenzene anion in function of various normal modes. The potential curves rationalize well the observed excitation functions and this agreement confirms, in turn, the qualitative validity of the potential curves and the conclusions drawn from them. In particular, this combined experimental and theoretical approach reveals a dominant role of vibronic coupling on the ground and excited states of the chlorobenzene anion. Vibrations of b_2 symmetry, in particular the vibration I studied in more detail here, couple the low-lying π^* states b_1 and a_2 , leading to double-minimum potential curves. Vibrations of b_1 symmetry, in particular the vibrations x and y studied here, couple the b_1 π^* state and the a_1 $\sigma_{\text{C-Cl}}^*$ state, leading to very flat potential curves with respect to out-of-plane bending. Finally vibrations of a_2 symmetry, in particular the vibration w studied here, couples the a_2 π^* state with the $\sigma_{\text{C-Cl}}^*$ state, also leading to a very flat potential curve with respect to twisting of the anion around the axis of the C-Cl bond.

The shape of the π^* band in the spectra depends strongly upon the choice of the final vibrational channel used as a means of its observation. In general it appears to have two strongly overlapping components, around 0.8 and 1.2 eV. The lower is seen, at least weakly, in the excitation of all vibrations, the upper only in some channels. The selectivity appears to favor the ordering b_1 below a_2 at the geometry of neutral chlorobenzene, but the evidence is not entirely conclusive. The calculated potential curves indicate that the two π^* states are very intimately entangled by nuclear motion and that much of the observed band splitting is due to coupling by vibration and not necessarily by a difference of the electronic energies at the equilibrium geometry of neutral chlorobenzene, in agreement with the conclusion reached already in ref. 5. The strong vibronic coupling has generally the consequence of fast 'hopping' of the nuclei from one surface to another¹⁸ so that dissociation proceeds from both and the inherent ordering is not very relevant.

The onset of the Cl^- yield coincides with the first vibrational feature of the lowest π^* state in the excitation spectra. This amounts to an experimental evidence (within about 0.05 eV) of absence of an energy barrier in the dissociation path. This is surprising in view of the fact that dissociation from this state is symmetry forbidden in C_{2v} , justifying the concern of Asfandiarov *et al.*¹² as how to explain the unexpectedly efficient though symmetry forbidden dissociation. Our assignment of the electronic states of the anion does not support their proposition that the traditional assignment of the 0.8–1.4 eV and the

8 2.6 eV band should be reversed, however. Our work indicates that the explanation lies in strong vibronic coupling which lowers the symmetry of the anion and reduces the energy along the dissociation path to such a degree as to provide a channel without activation energy.

Acknowledgements

This research is part of project No. 2000-061543.00 of the Swiss National Science Foundation.

References

- 1 J.-M. Savkant, *Acc. Chem. Res.*, 1993, 26, 455.
- 2 J.-M. Savkant, *Tetrahedron*, 1994, 50, 10117.
- 3 C. Costentin, P. Hapiot, M. Médebielle and J.-M. Savkant, *J. Am. Chem. Soc.*, 1999, 121, 4451.
- 4 K. D. Jordan and P. D. Burrow, *Acc. Chem. Res.*, 1978, 11, 341.
- 5 P. D. Burrow, A. Modelli and K. D. Jordan, *Chem. Phys. Lett.*, 1986, 132, 441.
- 6 T. Koopmans, *Physica*, 1934, 104, 1.
- 7 L. G. Asfandiarov, R. N. Compton, G. S. Hurst and P. W. Reinhardt, *J. Chem. Phys.*, 1966, 45, 536.
- 8 K. L. Stricklett, S. C. Chu and P. D. Burrow, *Chem. Phys. Lett.*, 1986, 131, 279.
- 9 R. Dressler, M. Allan and E. Haselbach, *Chimia*, 1985, 39, 385.
- 10 C. Bulliard, M. Allan and E. Haselbach, *J. Phys. Chem.*, 1994, 98, 11040.
- 11 D. D. Clarke and C. A. Coulson, *J. Chem. Soc. A*, 1969, 169.
- 12 N. L. Asfandiarov, V. S. Fal'ko, A. I. Fokin, O. G. Khvostenko, G. S. Lomakin, V. G. Lukin and E. P. Nafikova, *Rapid Commun. Mass Spectrosc.*, 2000, 141, 274.
- 13 A. Modelli and M. Venuti, *J. Phys. Chem. A*, 2001, 105, 5836.
- 14 I. V. Beregovaya and L. N. Shchegoleva, *Chem. Phys. Lett.*, 2001, 348, 501.
- 15 S. F. Wong and G. J. Schulz, *Phys. Rev. Lett.*, 1975, 35, 142.
- 16 L. Dubé and A. Herzenberg, *Phys. Rev. A*, 1975, 1, 1314.
- 17 I. Walker, S. F. Wong and A. Stamatović, *J. Chem. Phys.*, 1978, 69, 5532.
- 18 H. Estrada, L. S. Cederbaum and W. Domcke, *J. Chem. Phys.*, 1986, 84, 152.
- 19 M. Allan, *J. Phys. B*, 1992, 25, 1559.
- 20 M. Allan, *J. Phys. B*, 1995, 28, 5163.
- 21 M. Allan, *Phys. Rev. Lett.*, 2001, 87, 033201.
- 22 D. H. Whiffen, *J. Chem. Soc.*, 1956, 1350.
- 23 K. Rohr and F. Linder, *J. Phys. B*, 1976, 9, 2521.
- 24 M. Allan, N. C. Craig and L. V. McCarty, *J. Phys. B*, 2002, 35, 523.
- 25 D. Chen and G. A. Gallup, *J. Chem. Phys.*, 1990, 93, 8893.
- 26 T. Sommerfeld, *J. Am. Chem. Soc.*, 2002, 124, 1119.
- 27 A. Herzenberg, in: *Electron-Molecule Collisions*, ed. I. Shimamura and K. Takayanagi, Plenum Press, New York and London, 1984, p. 191.
- 28 M. Čížek, J. Horáček and W. Domcke, *J. Phys. B*, 1998, 31, 2571.
- 29 Ch. Bulliard, PhD Thesis, University of Fribourg, 1994.
- 30 M. Allan, *Helv. Chim. Acta*, 1982, 65, 2008.
- 31 Drawn with the program MOPLOT, T. Bally, B. Albrecht, S. Matzinger and G. M. Sastry, <http://www-chem.unifr.ch/pc/introduction/moplot.html>.
- 32 G. A. Gallup, *J. Chem. Phys.*, 1993, 99, 827.